

Precise scaling relations for self-interacting bosonic dark matter stars

Zhaorui Zhang,¹ Xudong Wang,^{2,*} and Bin Qi^{2,†}

¹*School of Space Science and Technology, Shandong University, Weihai 264209*

²*Shandong Provincial Key Laboratory of Nuclear Science,
Nuclear Energy Technology and Comprehensive Utilization,
Weihai Frontier Innovation Institute of Nuclear Technology, School of Nuclear Science,
Energy and Power Engineering, Shandong University, Shandong 250061, China*

The structural properties of bosonic dark matter stars are systematically investigated, presenting precise scaling relations for the mass, radius, central density, and the properties of dark matter particles. The dark matter equation of state is derived from a complex scalar field theory with a quartic self-interaction potential $V(\phi) = \frac{\lambda}{4}|\phi|^4$, considering boson masses m_ϕ ranging from 10^{-9} to 10^3 GeV and self-coupling constants λ ranging from 0.01π to 100π . The scaling relation for the maximum mass of bosonic dark matter stars, the corresponding critical radius and critical central density are obtained as

$$M_{\max} = 0.1 \frac{\sqrt{\lambda}}{m_\phi^2} M_\odot, \quad R(M_{\max}) = 0.9 \frac{\sqrt{\lambda}}{m_\phi^2} \text{ km}, \quad \varepsilon_{\max} = 2.1 \times 10^5 \frac{m_\phi^4}{\lambda} \text{ MeV/fm}^3,$$

where m_ϕ is in GeV, the relations for $R(M_{\max})$ and ε_{\max} are first put forward. The fitting relative error is less than 4%. Based on these scaling relations, we further provide global analytical fits for the stable branch. The relationships between mass and central density as well as radius and central density can be described by a unified function of the form:

$$\tilde{Y} = \frac{A}{[1 + (5\tilde{\varepsilon})^h]^s},$$

where for $Y = M$, $\tilde{M} \equiv M/M_{\max}$, $A = 1$, $h = -2$, $s = 0.42$; for $Y = R$, $\tilde{R} \equiv R/R(M_{\max})$, $A = 1.634$, $h = 1$, $s = 0.28$; and $\tilde{\varepsilon} \equiv \varepsilon_0/\varepsilon_{\max}$. The fitting relative error is less than 0.1%. Furthermore, we find a simple quadratic polynomial mass-radius relation for bosonic dark matter stars.

The remarkable similarity of scaled stellar configurations across vastly different parameter ranges might imply an underlying mathematical structure. These analytical scaling relations establish direct connections between the macroscopic properties of dark matter stars and the microscopic properties of dark matter particles, enabling researchers to quickly obtain stellar configurations without repeated numerical calculations.

I. INTRODUCTION

Dark matter is one of the central issues in contemporary physics and astrophysics. A large body of astrophysical and cosmological observational evidence, ranging from galaxy rotation curves and cluster dynamics to anisotropies in the cosmic microwave background radiation, strongly indicates the existence of a component of matter that cannot be detected through standard electromagnetic radiation [1–4]. The latest observations from the Planck satellite precisely determine that dark matter accounts for approximately 26.4% of the total energy density of the universe [5]. However, the microscopic particle nature of dark matter remains an unsolved mystery. Although weakly interacting massive particles have long been considered the most attractive candidates, decades of direct and indirect detection experiments have yet to provide conclusive evidence for their existence [6, 7]. This situation has led the community to turn attention to other dark matter candidates, including axions, ultralight scalar fields, and primordial black holes [8–10].

Among the many alternative models, scalar field dark matter that can form macroscopic compact objects through gravitational binding—namely boson stars—has received widespread attention [11, 12]. Wheeler first pointed out that a free complex scalar field without self-interaction can form gravitationally bound stable configurations [13]. Subsequently, Kaup and Ruffini established the basic theoretical framework for boson stars [11, 12]. For "mini-boson stars" composed of free complex scalar fields, the maximum mass is inversely proportional to the boson mass m_ϕ ,

* xudongwang@mail.sdu.edu.cn

† bqi@sdu.edu.cn

i.e., $M_{\max} \sim 1/m_\phi$ [11]. Under typical particle mass scales, this mass is far smaller than the Chandrasekhar limit, the maximum mass achievable by fermionic stars supported by degeneracy pressure [14], thus lacking astrophysical significance. To overcome this limitation, self-interactions are introduced to generalize the form of the potential, providing additional pressure to resist gravitational collapse [15, 16]. Colpi, Shapiro, and Wasserman systematically studied boson stars with a quartic self-interaction potential $V(\phi) = \lambda/4|\phi|^4$ [17]. They found that repulsive self-interactions dominate the pressure in dense regions, leading to a scaling $M_{\max} \sim \lambda^{1/2}/m_\phi^2$ for the maximum mass, which can reach or even exceed the mass scale of supermassive black holes when λ is sufficiently large. They further pointed out that the maximum mass of such self-interacting boson stars can be compared to the Chandrasekhar mass of fermions with mass $m_f \sim \lambda^{-1/4}m_\phi$, and that self-interaction effects remain non-negligible even for $\lambda \ll 1$ [17]. In their classic review, Schunck and Mielke further noted that self-interactions not only increase the maximum mass but also endow boson stars with structured layered features—including an anisotropic scalar matter core, an exponentially decaying "halo," and a completely regular spacetime geometry—making them a potential new type of compact object. Giant boson stars can also contribute to galaxy rotation curves, providing a natural explanation for dark matter [15]. Liebling and Palenzuela systematically summarized various subtypes of boson stars and their dynamical properties, emphasizing that boson stars with repulsive self-interactions, due to their significantly enhanced dynamical stability, are widely used as dark matter sources and black hole mimickers, with rich phenomenological implications in high-energy astrophysics [18–20]. Recent studies have further confirmed that self-interactions can effectively suppress the dynamical instability of scalar boson stars [21], while Bose-Einstein condensates with repulsive self-interactions can form stable solitonic structures on galactic scales, providing a microscopic foundation for dark matter models [22].

This paper focuses on the boson star model with a quartic self-interaction potential $V(\phi) = \frac{\lambda}{4}|\phi|^4$. Although the scaling relation $M_{\max} \propto \sqrt{\lambda}/m_\phi^2$ for the maximum mass has been known since the work of Colpi et al. [17], several important aspects remain unexplored. First, the numerical coefficients in these scaling relations have not been determined with high precision. Second, the scaling relation for the critical radius $R(M_{\max})$ and its connection to the maximum mass have not been systematically quantified. Third, and most importantly, although previous work has pointed out the existence of scaling properties in boson stars [35], high-precision analytical fitting formulas for the $M-\varepsilon_0$, $R-\varepsilon_0$, and $M-R$ relations over the entire stable branch have not yet appeared in the literature. The theoretical tool for studying boson star structure is the Tolman-Oppenheimer-Volkoff equation in the framework of general relativity [24, 25]. However, numerically solving the TOV equations typically requires re-integration for each set of parameters (m_ϕ, λ) , which hinders rapid theoretical predictions and astronomical data analysis. Therefore, finding universal analytical formulas describing the mass-radius-central density relations of boson stars has become an important task with significant practical value. Similar scaling relations have been explored in studies of neutron stars and quark stars [28, 31].

Through systematic scanning of a wide parameter space of (m_ϕ, λ) , we obtain precise scaling relations for the maximum mass, critical radius, and critical central density of boson stars, and present for the first time unified analytical fits for the $M-\varepsilon_0$, $R-\varepsilon_0$, and $M-R$ relations over the entire stable branch. These analytical formulas allow researchers to quickly obtain stellar configurations for arbitrary parameter combinations without repeated numerical calculations, providing a convenient tool for subsequent astrophysical applications and observational constraints.

This paper is organized as follows. Section II introduces the bosonic dark matter model and equation of state. Section III analyzes the behavior of the equation of state. Section IV presents the numerical solutions of the TOV equations and the structure of boson stars. Section V establishes the precise scaling relations at the extremal points. Section VI presents global analytical fits for the $M-\varepsilon_0$, $R-\varepsilon_0$, and $M-R$ relations. Section VII applies these relations to constrain Sgr A*. Finally, Section VIII summarizes our findings and outlines future work.

II. MODEL AND EQUATION OF STATE

A. Bosonic Dark Matter Model

We consider a bosonic dark matter model described by a complex scalar field ϕ with self-interaction. The Lagrangian density of the system is

$$\mathcal{L} = -\frac{1}{2}g^{\mu\nu}\phi_{;\mu}^*\phi_{;\nu} - \frac{1}{2}m_\phi^2|\phi|^2 - \frac{1}{4}\lambda|\phi|^4, \quad (1)$$

where m_ϕ is the boson mass and λ is the dimensionless self-coupling constant. When $\lambda > 0$, the self-interaction is repulsive, favoring the formation of more massive compact objects [17].

Under the mean-field approximation, the energy-momentum tensor of the system can be approximated as that of an ideal fluid, and anisotropies can be neglected [17]. Through mean-field treatment, the equation of state of the

system can be obtained [23]:

$$p = \frac{m_\phi^4 c^5}{9\lambda\hbar^3} \left(\sqrt{1 + \frac{3\lambda\hbar^3\varepsilon}{m_\phi^4 c^5}} - 1 \right)^2. \quad (2)$$

This equation of state exhibits two important asymptotic behaviors. In the low-energy density limit, $\frac{3\lambda\hbar^3\varepsilon}{m_\phi^4 c^5} \ll 1$, Eq. (2) can be approximated as

$$p \approx \frac{\lambda\hbar^3}{4m_\phi^4 c^5} \varepsilon^2, \quad (3)$$

exhibiting a soft quadratic behavior. In the high-energy density limit, $\frac{3\lambda\hbar^3\varepsilon}{m_\phi^4 c^5} \gg 1$, Eq. (2) approaches

$$p \approx \frac{\varepsilon}{3}, \quad (4)$$

the radiation-dominated linear equation of state.

B. TOV Equation

For static spherically symmetric compact objects, Einstein's field equations yield the Tolman-Oppenheimer-Volkoff equations describing hydrostatic equilibrium [24, 25]:

$$\frac{dp}{dr} = -\frac{G(\varepsilon + p/c^2)(M + 4\pi r^3 p/c^2)}{r^2(1 - 2GM/c^2 r)}, \quad (5)$$

$$\frac{dM}{dr} = 4\pi r^2 \varepsilon/c^2, \quad (6)$$

where $M(r)$ is the total mass enclosed within radius r , satisfying the boundary condition $M(0) = 0$. The stellar surface is defined by the condition $p(R) = 0$, and the total mass of the star is $M = M(R)$, with R being the stellar radius.

We numerically solve Eqs. (5)-(6) together with the equation of state (2) to compute the structure of boson stars for different parameters. To improve computational efficiency and cover a wide range of radial scales, we use a logarithmic grid from $r_{\min} = 10^{-22}$ m to $r_{\max} = 10^{22}$ m with $N = 20000$ grid points. The integration proceeds outward from the center and terminates when the pressure becomes negative (considered as reaching the stellar surface).

III. EQUATION OF STATE BEHAVIOR ANALYSIS

To comprehensively analyze the behavior of the equation of state (2), we first study its variation with parameters. We select three typical self-coupling constants $\lambda = 0.01\pi, \pi, 100\pi$, covering the entire range from weak to strong coupling. For each λ , we calculate the pressure-energy density relation for different boson masses $m_\phi = 10^{-9}, 10^{-6}, 10^{-3}, 1, 10^3$ GeV.

Figure 1 displays the equation of state, from which two important features can be observed:

First, for a fixed self-coupling constant λ , the equation of state becomes significantly softer as the boson mass m_ϕ increases. This means that at the same energy density, heavier bosons produce less pressure, making the resulting compact object more easily compressed. This behavior can be understood from the low-energy approximation in Eq. (3): the pressure is proportional to m_ϕ^{-4} , so larger mass implies smaller pressure.

Second, for a fixed boson mass m_ϕ , the equation of state in the low-energy density region becomes significantly stiffer as the self-coupling constant λ increases, while in the high-energy density region, curves for different λ gradually converge. This reflects the dual role of self-interaction: in the low-density region, repulsive self-interaction provides additional pressure support; in the high-density region, the radiation limit $p \approx \varepsilon/3$ dominates and is independent of λ .

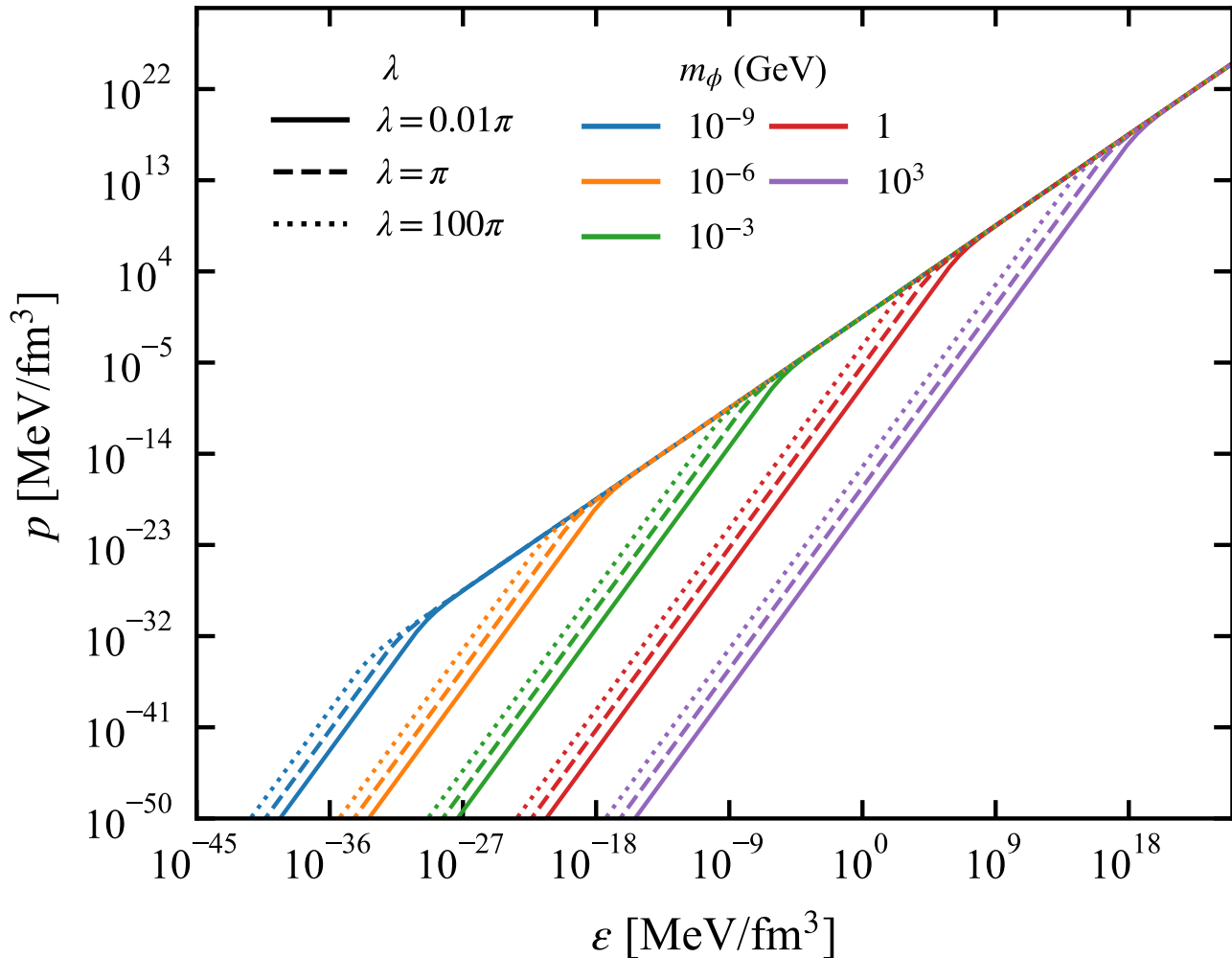


FIG. 1. Equation of state for self-interacting bosonic dark matter with a quartic potential. The figure shows the pressure p as a function of energy density ε for different boson masses m_ϕ (colors) and self-coupling constants λ (line styles). At low energy densities, the equation of state exhibits a soft quadratic behavior $p \propto \varepsilon^2$, while at high energy densities it asymptotes to the radiation-dominated limit $p = \varepsilon/3$.

IV. STRUCTURE OF BOSON STARS

Having analyzed the equation of state behavior of self-interacting bosonic dark matter in the previous section, we now systematically study the structural properties of boson stars described by this equation of state by numerically solving the Tolman-Oppenheimer-Volkoff equations in general relativity. We focus on the $M-\varepsilon_0$ and $R-\varepsilon_0$ relations as well as the $M-R$ relation of boson stars.

Specifically, we choose boson masses $m_\phi = 10^{-9}, 10^{-6}, 10^{-3}, 1, 10^3$ GeV, covering the entire range from ultralight to heavy masses. The self-coupling constant λ takes three typical values 0.01π , π , and 100π , corresponding to weak, moderate, and strong coupling regimes, respectively. For each set of parameters (m_ϕ, λ) , we obtain a family of boson star solutions by varying the central energy density ε_0 . For ease of expression, we refer to the radius $R(M_{\max})$ and central energy density ε_{\max} corresponding to the maximum mass M_{\max} as the **critical radius** and **critical central density**, respectively.

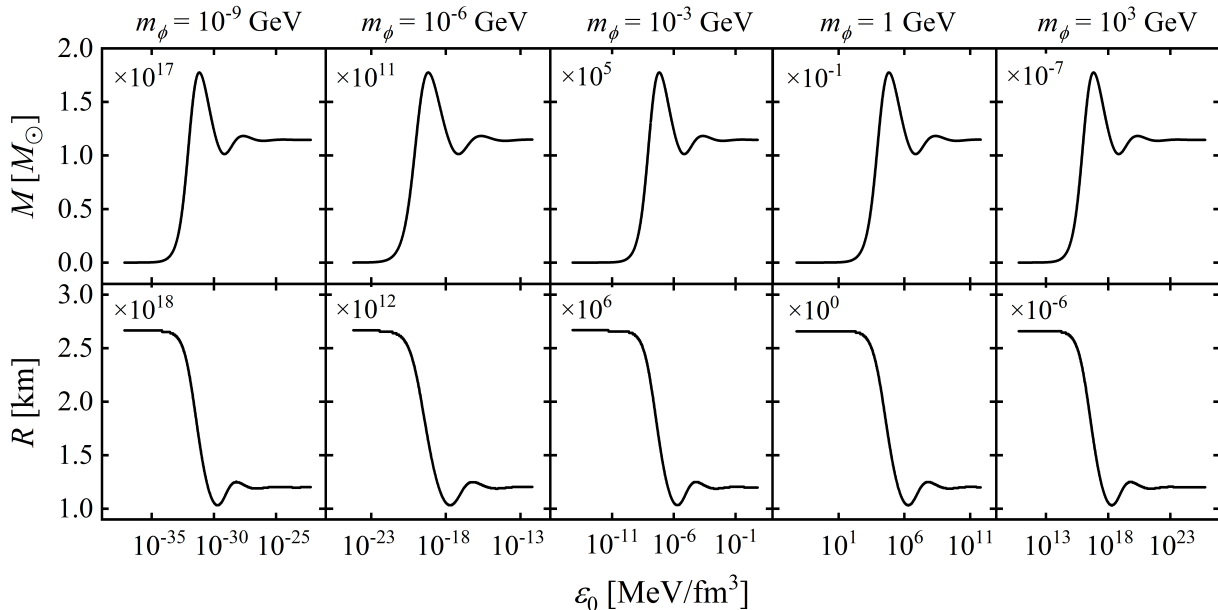


FIG. 2. Fixed $\lambda = \pi$, variation of boson star mass and radius with central energy density for different m_ϕ . From left to right: $m_\phi = 10^{-9}$, 10^{-6} , 10^{-3} , 1 , 10^3 GeV. Upper panels: M (in M_\odot) as a function of ε_0 ; lower panels: R (in km) as a function of ε_0 , with ε_0 in units of MeV/fm^3 .

A. Boson Star Structure for Different Mass Parameters

First, we fix the self-coupling constant $\lambda = \pi$ and study the variation of boson star structure with the mass parameter m_ϕ . Figure 2 shows the structural properties of boson stars for different mass parameters at $\lambda = \pi$, with each subfigure containing two panels displaying the M - ε_0 and R - ε_0 relations.

From the upper panels of Fig. 2 (the M - ε_0 relation), we see that each M - ε_0 curve has a maximum mass M_{max} . Before reaching the maximum, the mass increases monotonically with central density, corresponding to the stable equilibrium branch; after exceeding the maximum, the mass decreases with increasing central density and exhibits oscillations, corresponding to the unstable branch [26, 27]. In this paper, the stable branch is defined as the region $\varepsilon_0 \leq \varepsilon_{\text{max}}$, i.e., configurations where the central energy density does not exceed the critical central density ε_{max} . Configurations on the stable branch satisfy the standard radial perturbation hydrostatic stability criterion $\partial M / \partial \varepsilon_0 > 0$ [26]. This behavior is similar to that of ordinary neutron stars and is a universal feature of compact objects in general relativity, marking the limit of balance between gravity and repulsive forces (quantum pressure and self-interaction pressure).

The figure also shows that as the boson mass m_ϕ increases, the maximum mass decreases significantly and the corresponding critical central density shifts to higher values. For example, when $m_\phi = 10^{-9}$ GeV, the maximum mass can reach $M_{\text{max}} \sim 10^{17} M_\odot$; when $m_\phi = 10^3$ GeV, the maximum mass drops to $M_{\text{max}} \sim 10^{-7} M_\odot$, only of the order of Earth's mass. This behavior can be understood from the low-energy approximation of the equation of state: in the low-density region, $p \propto \lambda \varepsilon^2 / m_\phi^4$, the pressure is proportional to m_ϕ^{-4} , so heavier particles produce less pressure and consequently support smaller stellar masses.

Next, examine the lower panels of Fig. 2 (the R - ε_0 relation). The radius at the maximum mass on each R - ε_0 curve is denoted $R(M_{\text{max}})$, i.e., the critical radius. In the low-density region, the radius decreases with increasing central density; in the high-density region, the radius remains nearly constant after small oscillations.

The figure also shows that as m_ϕ increases, the critical radius $R(M_{\text{max}})$ decreases significantly. For $m_\phi = 10^{-9}$ GeV, the maximum mass radius can reach $R(M_{\text{max}}) \sim 10^{18}$ km, while for $m_\phi = 10^3$ GeV, the critical radius is only $R(M_{\text{max}}) \sim 10^{-6}$ km.

Figure 3 shows the mass-radius relation of boson stars for the same parameters, which is one of the most direct observables of compact objects and a key bridge connecting theoretical models with astronomical observations [28].

An important characteristic quantity can be extracted from Fig. 3—the critical radius $R(M_{\text{max}})$. For $m_\phi = 10^{-9}$ GeV, the maximum mass can reach $M_{\text{max}} \sim 10^{17} M_\odot$, with a corresponding critical radius of approximately

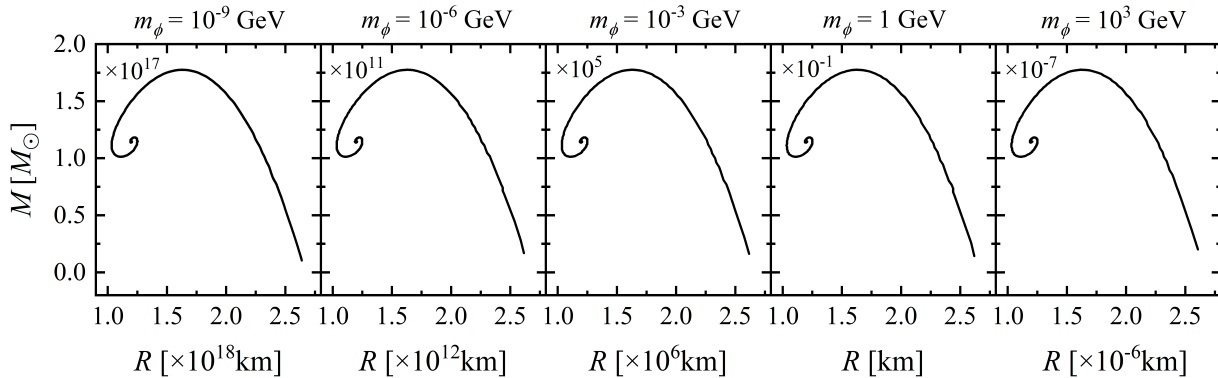


FIG. 3. Fixed self-coupling constant $\lambda = \pi$, mass-radius relation of boson stars for different boson masses m_ϕ . From left to right: $m_\phi = 10^{-9}, 10^{-6}, 10^{-3}, 1, 10^3$ GeV. Horizontal axis: radius R in km; vertical axis: mass M in solar masses M_\odot . Each curve is obtained by varying the central energy density ε_0 .

$R(M_{\max}) \sim 10^{18}$ km. This indicates that ultralight bosons can form supermassive compact objects, providing theoretical support for the dark matter origin hypothesis of supermassive compact objects such as Sgr A* at the Galactic center.

B. Boson Star Structure for Different Coupling Constants

Next, we fix the mass parameter $m_\phi = 1$ GeV and study the variation of boson star structure with the self-coupling constant λ . Figure 4 shows the $M-\varepsilon_0$ and $R-\varepsilon_0$ relations for different self-coupling constants, and Fig. 5 shows the corresponding mass-radius relations.

From the upper panels of Fig. 4 (the $M-\varepsilon_0$ relation), we see that as λ increases, the maximum mass increases significantly and the corresponding critical central density shifts to lower values. This indicates that stronger self-interaction provides greater repulsive pressure, thus supporting larger stellar masses.

From the lower panels of Fig. 4 (the $R-\varepsilon_0$ relation), we observe that as λ increases, the critical radius $R(M_{\max})$ also increases accordingly. At $\lambda = 0.01\pi$, the critical radius is approximately 0.17 km, while at $\lambda = 100\pi$, it reaches about 17 km.

From the mass-radius relations in Fig. 5, we find that as λ increases, the $M-R$ curves shift upward and rightward, indicating that strongly coupled boson stars have larger radii for the same mass. In the weak coupling regime, the maximum mass of boson stars is relatively small, $M_{\max} \approx 1.77 \times 10^{-2} M_\odot$; under moderate coupling, the maximum mass increases to $M_{\max} \approx 0.17 M_\odot$; in the strong coupling regime, the maximum mass further increases to $M_{\max} \approx 1.7 M_\odot$.

V. PRECISE SCALING RELATIONS AT EXTREMAL POINTS

A. Scaling Relation for the Maximum Mass

Through systematic analysis of the maximum mass for different parameters, we discover precise scaling relations. Figure 6 shows the variation of the maximum mass with boson mass for fixed self-coupling constant λ , where the solid line represents the theoretical scaling relation $M_{\max} = 0.1\sqrt{\lambda}/m_\phi^2$, and the discrete points are numerical results from solving the TOV equations.

Figure 6 clearly shows perfect agreement between numerical points and theoretical curves. On a log-log scale, M_{\max} exhibits a strict power-law relation with m_ϕ , with a fitted slope of approximately -2.00 ± 0.01 , i.e.,

$$M_{\max} \propto m_\phi^{-2}. \quad (7)$$

This scaling relation can be understood from the low-energy asymptotic form of the equation of state: when ε is small, $p \propto \lambda\varepsilon^2/m_\phi^4$, and dimensional analysis yields $M \propto m_\phi^{-2}$ [17].

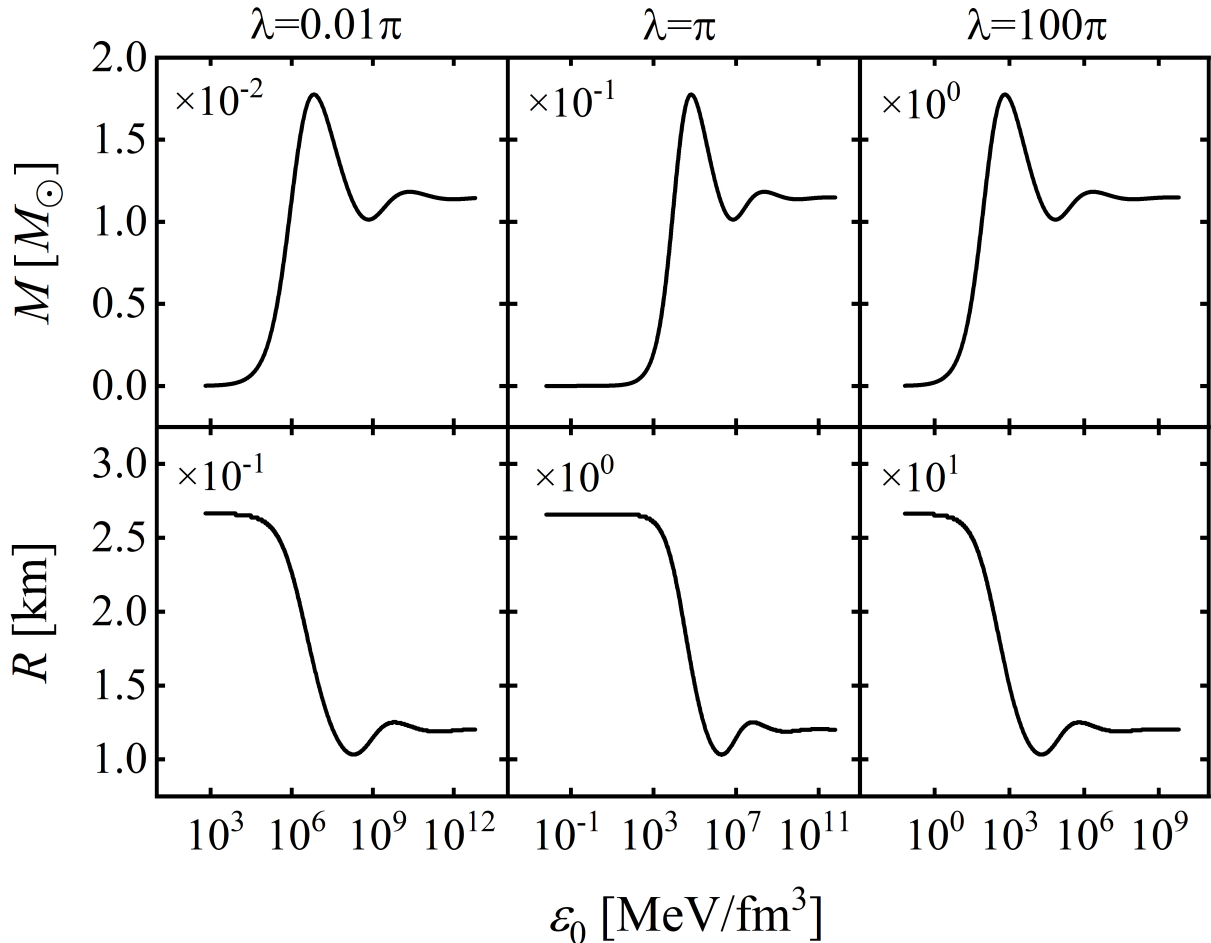


FIG. 4. Fixed mass $m_\phi = 1$ GeV, variation of boson star mass and radius with central energy density for different self-coupling constants λ . From left to right: $\lambda = 0.01\pi$, π , 100π . Upper panels: M (in M_\odot) as a function of ε_0 ; lower panels: R (in km) as a function of ε_0 , with ε_0 in units of MeV/fm^3 .

Similarly, fixing the boson mass m_ϕ and varying the self-coupling constant λ in numerical calculations, we find that the maximum mass M_{max} is proportional to $\sqrt{\lambda}$, i.e.,

$$M_{\text{max}} \propto \lambda^{1/2}. \quad (8)$$

This behavior reflects the supporting role of repulsive self-interaction on stellar structure: the larger λ is, the greater the additional pressure provided, and the larger the maximum mass that can be supported.

Combining these two scaling relations, the maximum mass can be uniformly expressed as

$$M_{\text{max}} = 0.1 \frac{\sqrt{\lambda}}{m_\phi^2}, \quad (9)$$

with m_ϕ in units of GeV and M_{max} in solar masses M_\odot .

B. Scaling Relation for the Critical Radius

For compact object research, the critical radius $R(M_{\text{max}})$ is another important physical quantity. We systematically analyze this quantity as well. Figure 7 shows the variation of $R(M_{\text{max}})$ with m_ϕ for fixed λ , with solid lines representing

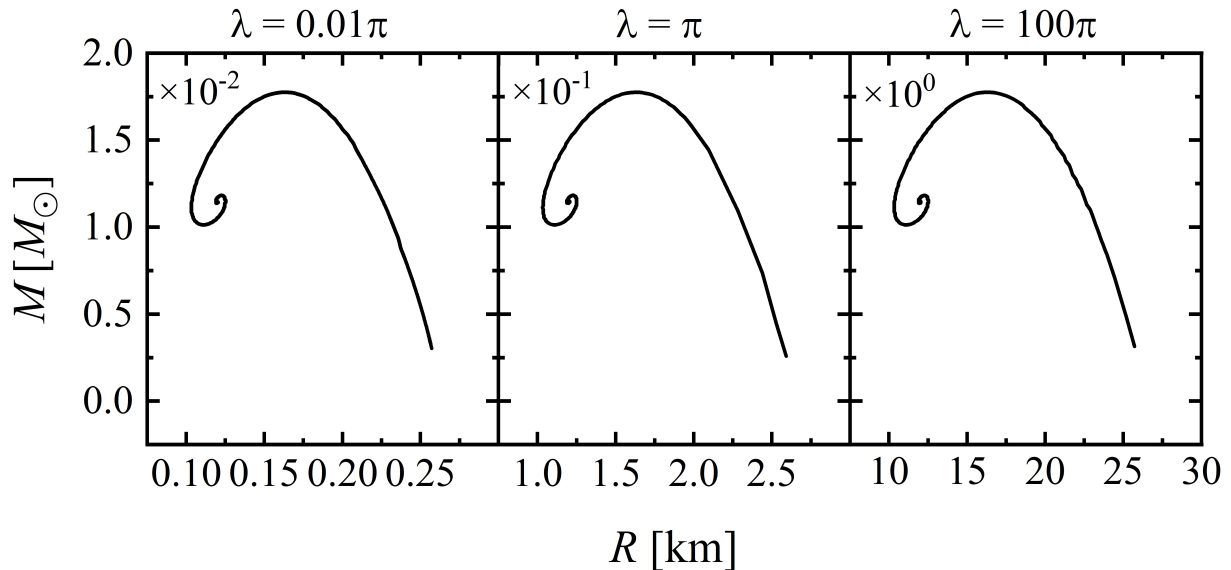


FIG. 5. Fixed mass $m_\phi = 1$ GeV, mass-radius relation of boson stars for different self-coupling constants λ . From left to right: $\lambda = 0.01\pi$, π , 100π . Horizontal axis: radius R in km; vertical axis: mass M in solar masses M_\odot . Each curve is obtained by varying the central energy density ε_0 .

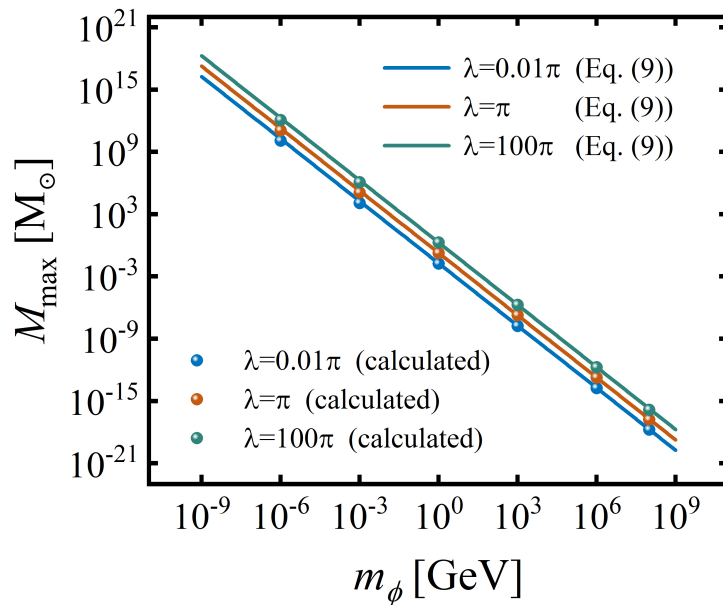


FIG. 6. Fixed self-coupling constant λ , variation of maximum mass M_{\max} with boson mass m_ϕ . Solid lines represent the theoretical scaling relation Eq. (9), where blue, red, and green correspond to $\lambda = 0.01\pi$, π , and 100π , respectively. Discrete points are numerical results from solving the TOV equations.

the theoretical scaling relation and discrete points being TOV numerical solutions.

The analysis results show that the critical radius $R(M_{\max})$ exhibits exactly the same scaling behavior with m_ϕ and

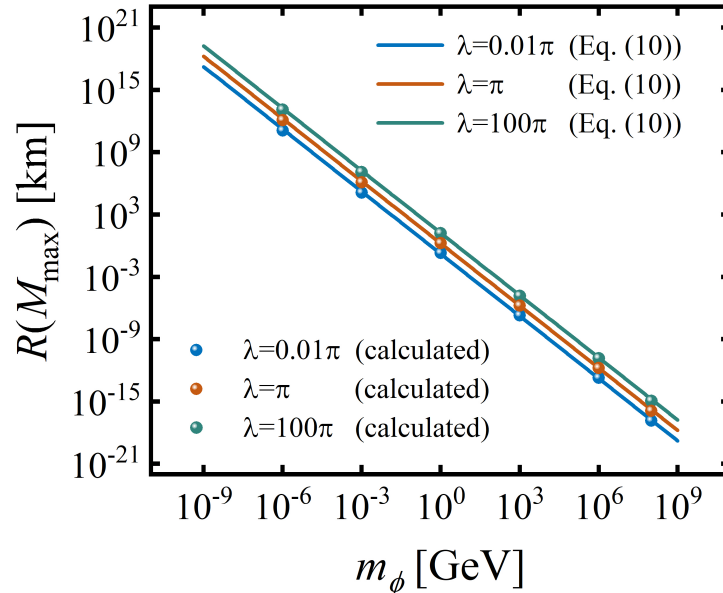


FIG. 7. Fixed self-coupling constant λ , variation of critical radius $R(M_{\max})$ with boson mass m_ϕ . Solid lines represent the theoretical scaling relation Eq. (10), with different colors corresponding to different λ values. Discrete points are numerical results from solving the TOV equations.

λ as the maximum mass M_{\max} :

$$R(M_{\max}) = 0.9 \frac{\sqrt{\lambda}}{m_\phi^2}, \quad (10)$$

with $R(M_{\max})$ in km. It is noteworthy that M_{\max} and $R(M_{\max})$ have identical dependencies on m_ϕ and λ , reflecting the self-similarity of compact stellar structures.

From Eqs. (9) and (10), the ratio of the maximum mass to the critical radius for the same (m_ϕ, λ) combination is a universal constant:

$$\frac{M_{\max}}{R(M_{\max})} = \frac{1}{9} \frac{M_\odot}{\text{km}}. \quad (11)$$

That is, $M_{\max} = \frac{1}{9} R(M_{\max})$. Linear fitting of the data yields a slope of 1.00006 ± 0.00004 ($R^2 > 0.9999$, where R^2 denotes the coefficient of determination), confirming $M_{\max} \propto R(M_{\max})$ and the ratio $M_{\max}/R(M_{\max}) \approx \frac{1}{9}$, with error less than 2%.

From the scaling relations, we can further obtain the compactness of the boson star at the critical point:

$$C \equiv \frac{GM_{\max}}{R(M_{\max})c^2} = \frac{G}{c^2} \cdot \frac{1}{9} \frac{M_\odot}{\text{km}} = 0.164. \quad (12)$$

This value is comparable in magnitude to the compactness of neutron stars, indicating that boson stars with quartic self-interaction are also highly compact at the maximum mass.

C. Scaling Relation for the Critical Central Density

The critical central density ε_{\max} also exhibits universal scaling behavior. Starting from the low-energy approximation of the equation of state $p \propto \lambda \varepsilon^2 / m_\phi^4$, dimensional analysis gives

$$\varepsilon_{\max} = 2.1 \times 10^5 \frac{m_\phi^4}{\lambda}, \quad (13)$$

where ε_{\max} is in MeV/fm^3 and m_ϕ is in GeV , $R^2 > 0.9999$. This scaling relation is consistent with those for M_{\max} and $R(M_{\max})$: from Eqs. (9), (10), and (13), we can verify $M_{\max} \propto \sqrt{\lambda}/m_\phi^2 \propto 1/\sqrt{\varepsilon_{\max}}$, consistent with the universal scaling law for compact stars.

These three scaling relations form the theoretical foundation for subsequent studies of the macroscopic properties of boson stars and their comparison with astronomical observations.

VI. GLOBAL ANALYTICAL FITS

A. M - ε_0 and R - ε_0 Relations

In Section V, we established precise scaling relations for the maximum mass, critical radius, and critical central density. Based on these, we now present global analytical fits for the M - ε_0 and R - ε_0 relations over the entire stable branch. The stable branch is defined as configurations with central energy density not exceeding the critical central density ε_{\max} , satisfying the standard stability criterion $\partial M/\partial \varepsilon_0 > 0$ [26]. We find that these two relations can be described by a unified function of the form:

$$\tilde{Y} = \frac{A}{\left[1 + (5\tilde{\varepsilon})^h\right]^s}, \quad (14)$$

where for $Y = M$, $\tilde{M} \equiv M/M_{\max}$, $A = 1$, $h = -2$, $s = 0.42$; for $Y = R$, $\tilde{R} \equiv R/R(M_{\max})$, $A = 1.634$, $h = 1$, $s = 0.28$; and $\tilde{\varepsilon} \equiv \varepsilon_0/\varepsilon_{\max}$. These parameters remain constant over the entire parameter range $10^{-9} \leq m_\phi/\text{GeV} \leq 10^3$ and $0.01\pi \leq \lambda \leq 100\pi$. The fitting error of Eq. (14) over the entire stable branch is less than 0.1% with $R^2 > 0.9995$.

It should be noted that the parameters A , h , and s in the fitting formula are shape parameters whose numerical values do not carry independent physical significance. The precise maximum mass, critical radius, and critical central density should be calculated using Eqs. (9), (10), and (13), while Eq. (14) has the advantage of describing the entire stable branch with a unified dimensionless functional form. Based on the power-law form of the scaling relations and the self-similarity of the TOV equations, these fitting formulas can be reasonably extrapolated to other (m_ϕ, λ) combinations beyond the parameter range considered in this paper.

Several important physical features can be read from the fitting results:

1. Scaling relation for characteristic density: $\varepsilon_{\max} \propto m_\phi^4/\lambda$, together with $Y_{\max} \propto \sqrt{\lambda}/m_\phi^2$, reflects the self-similarity of the system.
2. Difference in shape parameters: for the mass fit $h = -2 < 0$ while for the radius fit $h = 1 > 0$, indicating that the contraction behavior of radius with central density and the growth behavior of mass have different functional characteristics, consistent with the trends observed in Figs. 2 and 4.
3. Variation of radius within the stable branch: for the radius fit, within the stable branch ($\varepsilon_0 \leq \varepsilon_{\max}$), when $\varepsilon_0 \ll \varepsilon_{\max}$, $\tilde{R} \approx A = 1.634$, i.e., $R \approx 1.634R(M_{\max})$; at the critical point, $\tilde{R} = 1$, i.e., $R = R(M_{\max})$. The radius varies by a factor of about 1.6, quantitatively characterizing the evolution of the boson star radius with increasing central density.

B. Universal Mass-Radius Relation

After scaling transformation using the scaling relations (9) and (10) with the maximum mass M_{\max} and critical radius $R(M_{\max})$, the dimensionless M - R curves for all parameter combinations collapse onto a single curve. Quadratic polynomial fitting of the stable branch data yields:

$$\tilde{M} = b_0 + b_1\tilde{R} + b_2\tilde{R}^2, \quad (15)$$

with coefficients

$$b_0 = -1.9, \quad b_1 = 5.6, \quad b_2 = -2.7. \quad (16)$$

This fit has been verified over multiple independent parameter combinations covering m_ϕ from 10^{-9} to 10^3 GeV and λ from 0.01π to 100π , spanning both weak and strong coupling regimes. The coefficients are very stable across the

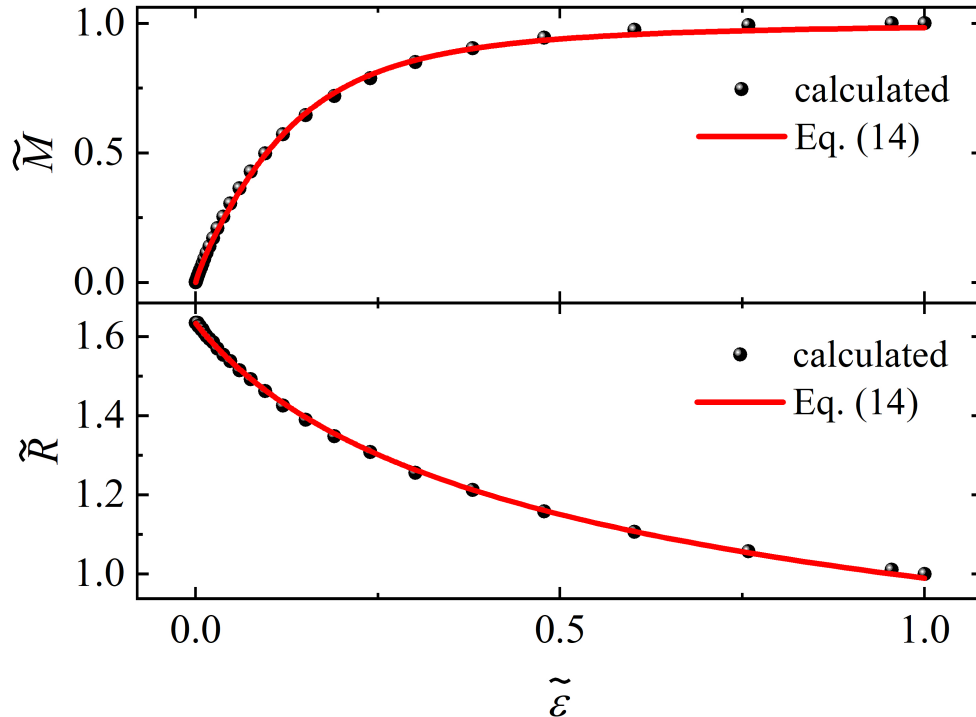


FIG. 8. Dimensionless mass \tilde{M} and radius \tilde{R} as functions of dimensionless central density $\tilde{\varepsilon}$ on the stable branch. Scattered points are numerically calculated results from the TOV equations, and the red solid curves are given by Eq. (14). For all parameter combinations (m_ϕ from 10^{-9} to 10^3 GeV, λ from 0.01π to 100π), the calculated results are almost identical. Upper panel: \tilde{M} - $\tilde{\varepsilon}$; lower panel: \tilde{R} - $\tilde{\varepsilon}$.

entire parameter space, with relative errors for all three parameters less than 3%. The R^2 for each set of parameters is > 0.9997 . This remarkable universality confirms the self-similar nature of boson star structure, suggesting an underlying mathematical structure worthy of further investigation.

Combining the scaling relations (9) and (10), Eq. (15) enables one to directly obtain the radius of a boson star for any given mass on the stable branch without solving the TOV equations, simply by calculating

$$M_{\max} = 0.1 \frac{\sqrt{\lambda}}{m_\phi^2} M_\odot, \quad R(M_{\max}) = 0.9 \frac{\sqrt{\lambda}}{m_\phi^2} \text{ km}, \quad (17)$$

and then solving for \tilde{R} from \tilde{M} using the inverse function of Eq. (15).

Equation (15) is valid within the range $\tilde{R} \lesssim 1.5$ (i.e., $\tilde{M} \gtrsim 0.5$), with a reproduction accuracy of $R^2 > 0.9995$ for the numerical results. The remarkable similarity of scaled stellar configurations across twelve orders of magnitude in boson mass and four orders of magnitude in self-coupling strength is an extraordinary discovery. It suggests that the universality found in this paper may extend beyond the specific quartic potential to a broader class of dark matter equations of state with similar scaling properties.

C. Definition of the Central Density Range

On the stable branch, as the central density decreases, the mass of the boson star decreases rapidly, and the gravitational binding weakens significantly. When $\tilde{\varepsilon} \ll 1$, the configuration mass is much smaller than M_{\max} , and the radius approaches its maximum $R \approx 1.634R(M_{\max})$, with an extremely weak surface gravitational field. In traditional compact object (neutron star, white dwarf) research, attention is typically focused on configurations near the maximum mass on the stable branch, as such configurations have sufficiently strong gravitational binding to be observed through X-rays, gravitational waves, etc. [28, 29]. For example, reviews of neutron star mass-radius relations

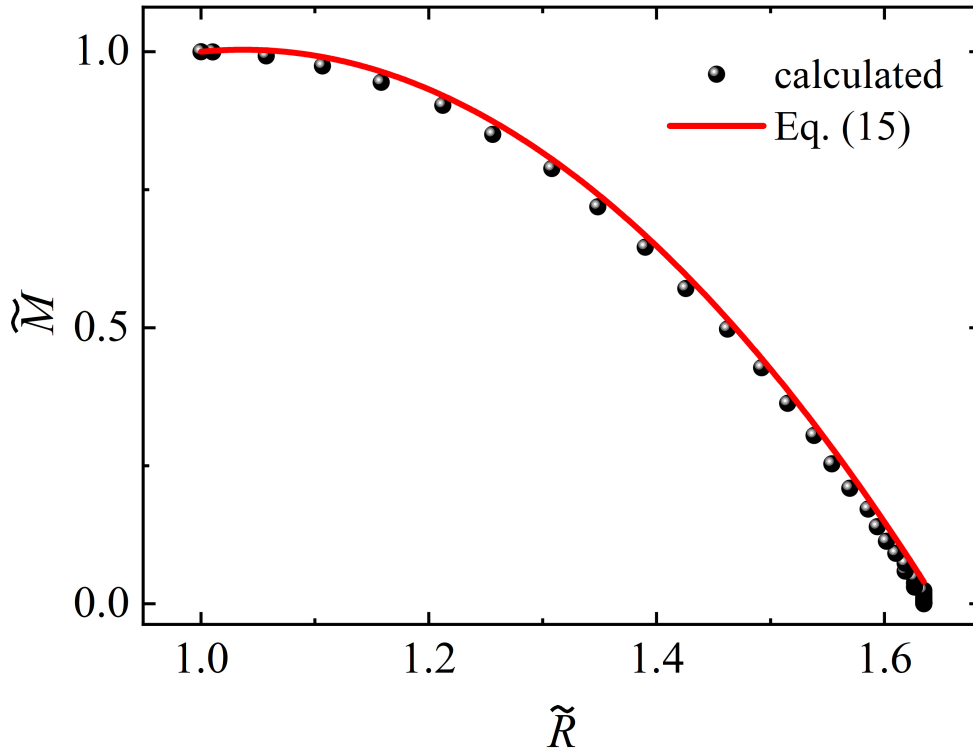


FIG. 9. Dimensionless mass-radius relation on the stable branch. Scattered points are numerically calculated results from the TOV equations, and the red solid curve is given by Eq. (15). For all parameter combinations (m_ϕ from 10^{-9} to 10^3 GeV, λ from 0.01π to 100π), the calculated results are almost identical.

focus on configurations near the maximum mass [30]. Based on the fitting accuracy analysis described above, this paper considers $\tilde{\varepsilon} \gtrsim 0.05$ (corresponding to $\tilde{M} \gtrsim 0.3$) as the central density range of primary astrophysical significance. Within this region, the accuracy of all analytical fitting formulas is better than 5%; for $\tilde{\varepsilon} < 0.05$, the boson star mass is less than 30% of the maximum mass, the gravitational binding is significantly weakened, and it is difficult to distinguish from dark matter halos or ordinary gas clouds with current observational capabilities. Therefore, this paper does not take such configurations as the main research object.

VII. BOSON STAR INTERPRETATION OF SGR A* AT THE GALACTIC CENTER

The compact radio source Sgr A* at the Galactic center is the closest massive compact object to Earth. Its mass has been precisely measured to be $(4.154 \pm 0.014) \times 10^6 M_\odot$ [32], corresponding to a Schwarzschild radius of approximately 1.27×10^7 km. Observations by the Event Horizon Telescope further reveal the shadow structure of Sgr A*, with an angular diameter of $48.7 \pm 7 \mu\text{as}$, corresponding to a linear scale of approximately 6.6×10^7 km [33, 34].

In this section, we use the scaling relations obtained in Section V to test whether Sgr A* can be interpreted as a boson star with quartic self-interaction.

For a stable boson star, its total mass M cannot exceed the maximum mass M_{max} , and its radius R cannot be smaller than the critical radius $R(M_{\text{max}})$. Therefore, the observational requirements for Sgr A* are

$$M_{\text{obs}} \leq M_{\text{max}}, \quad (18)$$

$$R_{\text{obs}} \geq R(M_{\text{max}}), \quad (19)$$

where $M_{\text{obs}} = 4.154 \times 10^6 M_\odot$ and $R_{\text{obs}} = 6.6 \times 10^7$ km.

Substituting the scaling relations (9) and (10) into the above inequalities yields

$$0.1 \frac{\sqrt{\lambda}}{m_\phi^2} \geq 4.154 \times 10^6, \quad (20)$$

$$0.9 \frac{\sqrt{\lambda}}{m_\phi^2} \leq 6.6 \times 10^7. \quad (21)$$

Thus, m_ϕ must satisfy

$$\sqrt{\frac{0.9}{6.6 \times 10^7}} \lambda^{1/4} \leq m_\phi \leq \sqrt{\frac{0.1}{4.154 \times 10^6}} \lambda^{1/4}, \quad (22)$$

We obtain

$$1.17 \times 10^{-4} \lambda^{1/4} \text{ GeV} \leq m_\phi \leq 1.55 \times 10^{-4} \lambda^{1/4} \text{ GeV}. \quad (23)$$

Converting to keV units ($1 \text{ GeV} = 10^6 \text{ keV}$):

$$117 \text{ keV} \leq \frac{m_\phi}{\lambda^{1/4}} \leq 155 \text{ keV}. \quad (24)$$

Equation (24) follows from the extremal conditions $M_{\text{obs}} \leq M_{\text{max}}$ and $R_{\text{obs}} \geq R(M_{\text{max}})$, which are necessary but not sufficient for the boson star interpretation—any viable configuration must simultaneously satisfy the M - ε_0 and R - ε_0 relations on the stable branch. A more stringent constraint is obtained by requiring that the observed mass and radius correspond to a specific point on the unified fitting formula (14). From Eqs. (14) and (11), the mass-to-radius ratio depends solely on the dimensionless central density $\tilde{\varepsilon}$:

$$\frac{M}{R} = \frac{M_{\text{max}}}{R(M_{\text{max}})} \frac{[1 + (5\tilde{\varepsilon})^{-2}]^{-0.42}}{1.634 [1 + 5\tilde{\varepsilon}]^{-0.28}}. \quad (25)$$

Substituting the observed values $M_{\text{obs}} = 4.154 \times 10^6 M_\odot$ and $R_{\text{obs}} = 6.6 \times 10^7 \text{ km}$, together with $M_{\text{max}}/R(M_{\text{max}}) = 1/9 M_\odot/\text{km}$ from Eq. (11), yields $\tilde{\varepsilon} \approx 0.207$. The corresponding dimensionless mass is $\tilde{M}(0.207) \approx 0.758$, from which $M_{\text{max}} = M_{\text{obs}}/\tilde{M} \approx 5.48 \times 10^6 M_\odot$. Combining this with the scaling relation $M_{\text{max}} = 0.1\sqrt{\lambda}/m_\phi^2$ from Eq. (9) gives

$$\frac{m_\phi}{\lambda^{1/4}} \approx 1.35 \times 10^{-4} \text{ GeV} = 135 \text{ keV}. \quad (26)$$

This value lies within the interval (23), confirming the self-consistency of the two approaches.

Figure 10 displays the allowed parameter space from the bounding conditions. The blue solid line represents the lower bound from the radius constraint $(m_\phi)_{\text{min}} = 1.17 \times 10^{-4} \lambda^{1/4} \text{ GeV}$, and the red solid line represents the upper bound from the mass constraint $(m_\phi)_{\text{max}} = 1.55 \times 10^{-4} \lambda^{1/4} \text{ GeV}$. The orange shaded region between the two boundaries is the parameter space consistent with Sgr A* observations; the refined value $m_\phi/\lambda^{1/4} = 1.35 \times 10^{-4} \text{ GeV}$ from Eq. (26) lies near the center of this region.

VIII. SUMMARY

This paper systematically investigates the structural properties of bosonic dark matter stars with a quartic self-interaction potential. Using the equation of state derived from the potential $V(\phi) = \frac{\lambda}{4}|\phi|^4$ and solving the TOV equations, we obtain precise scaling relations for the maximum mass, critical radius, and critical central density: $M_{\text{max}} = 0.1\sqrt{\lambda}/m_\phi^2 M_\odot$, $R(M_{\text{max}}) = 0.9\sqrt{\lambda}/m_\phi^2 \text{ km}$, $\varepsilon_{\text{max}} = 2.1 \times 10^5 m_\phi^4/\lambda \text{ MeV/fm}^3$, where m_ϕ is in GeV. The ratio $M_{\text{max}}/R(M_{\text{max}}) \approx 1/9 M_\odot/\text{km}$ is a universal constant, verified across all parameter combinations. Based on these scaling relations, we construct global analytical fits for the entire stable branch: the M - ε_0 and R - ε_0 relations can be described by the unified dimensionless function $\tilde{Y} = A/[1 + (5\tilde{\varepsilon})^h]^s$, with different (A, h, s) parameter sets for \tilde{M} and \tilde{R} ; the dimensionless mass-radius curve collapses to a single universal quadratic relation $\tilde{M} = -1.9 + 5.6\tilde{R} - 2.7\tilde{R}^2$. Applying these scaling relations to Sgr A* at the Galactic center, we obtain the constraint $117 \text{ keV} \leq m_\phi/\lambda^{1/4} \leq 155 \text{ keV}$, indicating that the self-interacting bosonic dark matter stars are viable candidates for Sgr A*.

This remarkable universality across twelve orders of magnitude in boson mass and four orders of magnitude in self-coupling strength suggests an underlying mathematical structure—likely rooted in the scaling symmetry of the

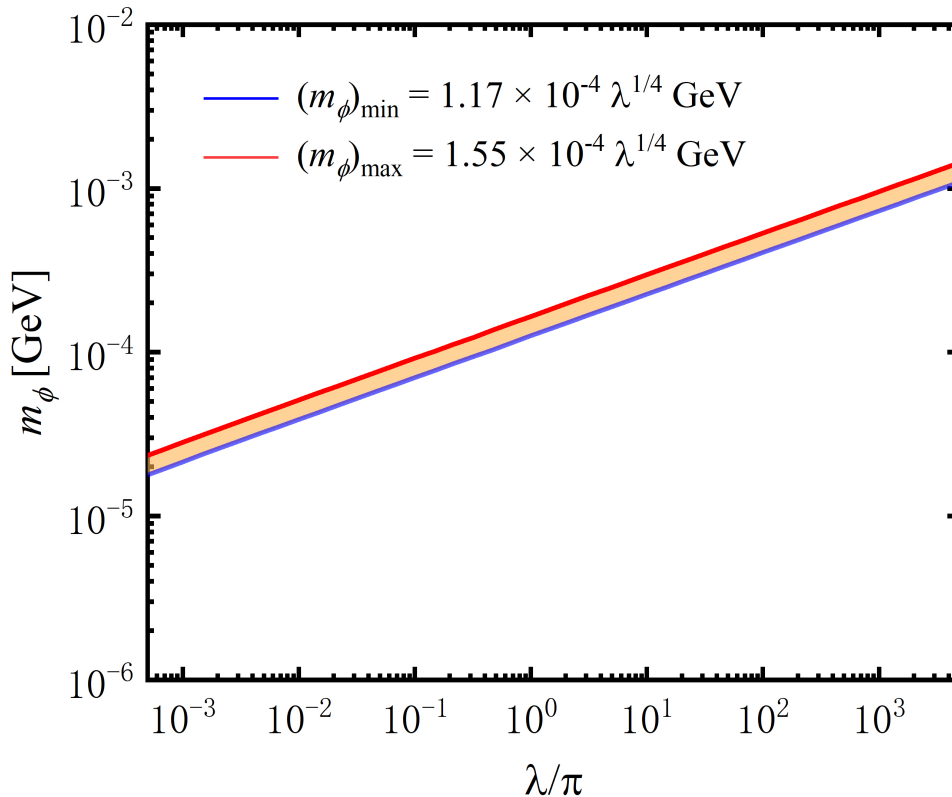


FIG. 10. Allowed parameter space for Sgr A* as a bosonic dark matter star. The blue solid line is the lower bound from the radius constraint $(m_\phi)_{\min} = 1.17 \times 10^{-4} \lambda^{1/4}$ GeV, and the red solid line is the upper bound from the mass constraint $(m_\phi)_{\max} = 1.55 \times 10^{-4} \lambda^{1/4}$ GeV. The orange shaded region between the two boundaries is the parameter space satisfying the observed mass ($4.154 \times 10^6 M_\odot$) and shadow size (6.6×10^7 km) of Sgr A*. Note that the combined parameter $m_\phi/\lambda^{1/4}$ is restricted to the narrow range $(1.17\text{--}1.55) \times 10^{-4}$ GeV.

Einstein-Klein-Gordon system—and may extend to a broader class of dark matter equations of state. The complete set of analytical formulas presented in this paper—the scaling relations for the maximum mass, critical radius, and critical central density, the unified fitting functions for $M(\varepsilon_0)$ and $R(\varepsilon_0)$, and the universal quadratic M – R relation—enables researchers to quickly obtain boson star configurations for arbitrary parameter combinations without repeated numerical integration of the TOV equations. Future higher-resolution EHT observations, GRAVITY stellar orbit monitoring, and next-generation dark matter detection experiments will further test the boson star hypothesis and the scaling relations reported in this paper.

ACKNOWLEDGMENTS

This work is partly supported by the National Natural Science Foundation of China (No. 12475123, No. 12225504, No.12321005).

-
- [1] G. Bertone, D. Hooper, and J. Silk, *Phys. Rep.* **405**, 279 (2005).
 - [2] G. Arcadi, M. Dutra, P. Ghosh, M. Lindner, Y. Mambrini, M. Pierre, S. Profumo, and F. S. Queiroz, *Eur. Phys. J. C* **78**, 203 (2018).
 - [3] M. Schumann, *J. Phys. G* **46**, 103003 (2019).

- [4] D. Clowe, M. Bradač, A. H. Gonzalez, M. Markevitch, S. W. Randall, C. Jones, and D. Zaritsky, *Astrophys. J. Lett.* **648**, L109 (2006).
- [5] Planck Collaboration, N. Aghanim *et al.*, *Astron. Astrophys.* **641**, A6 (2020).
- [6] D. S. Akerib *et al.* (LUX Collaboration), *Phys. Rev. Lett.* **118**, 021303 (2017).
- [7] E. Aprile *et al.* (XENON Collaboration), *Phys. Rev. Lett.* **121**, 111302 (2018).
- [8] D. J. E. Marsh, *Phys. Rep.* **643**, 1 (2016).
- [9] L. Hui, J. P. Ostriker, S. Tremaine, and E. Witten, *Phys. Rev. D* **95**, 043541 (2017).
- [10] A. M. Green and B. J. Kavanagh, *J. Phys. G* **48**, 043001 (2021).
- [11] D. J. Kaup, *Phys. Rev.* **172**, 1331 (1968).
- [12] R. Ruffini and S. Bonazzola, *Phys. Rev.* **187**, 1767 (1969).
- [13] J. A. Wheeler, *Phys. Rev.* **97**, 511 (1955).
- [14] S. Chandrasekhar, *Astrophys. J.* **74**, 81 (1931).
- [15] F. E. Schunck and E. W. Mielke, *Class. Quantum Grav.* **20**, R301 (2003).
- [16] P. Jetzer, *Phys. Rep.* **220**, 163 (1992).
- [17] M. Colpi, S. L. Shapiro, and I. Wasserman, *Phys. Rev. Lett.* **57**, 2485 (1986).
- [18] S. L. Liebling and C. Palenzuela, *Living Rev. Rel.* **15**, 6 (2012).
- [19] H. Olivares, Z. Younsi, C. M. Fromm, M. De Laurentis, O. Porth, Y. Mizuno, H. Falcke, M. Kramer, and L. Rezzolla, *Mon. Not. R. Astron. Soc.* **497**, 521 (2020).
- [20] F. H. Vincent, M. Wielgus, M. A. Abramowicz, E. Gourgoulhon, J.-P. Lasota, T. Paumard, and G. Perrin, *Astron. Astrophys.* **646**, A37 (2021).
- [21] V. Jaramillo and S.-Y. Zhou, *Complex structures of boson stars and anisotropic distribution of satellite galaxies*, arXiv:2407.12084 (2024).
- [22] P. H. Chavanis, *Phys. Rev. D* **107**, 103503 (2023).
- [23] P. H. Chavanis and T. Harko, *Phys. Rev. D* **86**, 064011 (2012).
- [24] R. F. Tooper, *Astrophys. J.* **140**, 434 (1964).
- [25] J. R. Oppenheimer and G. M. Volkoff, *Phys. Rev.* **55**, 374 (1939).
- [26] B. K. Harrison, K. S. Thorne, M. Wakano, and J. A. Wheeler, *Gravitation Theory and Gravitational Collapse* (University of Chicago Press, 1965).
- [27] J. M. Bardeen, K. S. Thorne, and D. W. Meltzer, *Astrophys. J.* **145**, 505 (1966).
- [28] J. M. Lattimer and M. Prakash, *Astrophys. J.* **550**, 426 (2001).
- [29] J. M. Lattimer and M. Prakash, *Science* **304**, 536 (2004).
- [30] J. M. Lattimer and M. Prakash, *Phys. Rep.* **442**, 109 (2007).
- [31] K. Yagi and N. Yunes, *Phys. Rep.* **681**, 1 (2017).
- [32] GRAVITY Collaboration, R. Abuter *et al.*, *Astron. Astrophys.* **657**, L12 (2022).
- [33] Event Horizon Telescope Collaboration, K. Akiyama *et al.*, *Astrophys. J. Lett.* **930**, L12 (2022).
- [34] Event Horizon Telescope Collaboration, K. Akiyama *et al.*, *Astrophys. J. Lett.* **930**, L13 (2022).
- [35] P. Agnihotri, J. Schaffner-Bielich, and I. N. Mishustin, *Phys. Rev. D* **79**, 084033 (2009).